A Next Generation Mm-Wave 2-Port MIMO Antenna Array with Wideband Characteristics for Wireless Applications

Kainat Ijaz, Shahid Bashir
Department of Electrical Engineering University of Engineering and Technology, Peshawar, Pakistan
*Correspondence: shahid.bashir@uetpeshawar.edu.pk

Citation | Ijaz. K, Bashir. S, "A Next Generation Mm-Wave 2-Port Mimo Antenna Array with Wideband Characteristics for Wireless Applications", IJIST, Vol. 8 Issue. 1 pp 51-68, January 2026
Received| December 01, 2025 **Revised|** December 28, 2025 **Accepted|** January 01, 2026
Published| January 07, 2026.

Fifth-generation (5G) technology is attracting significant interest because of its advanced features and its capability to tackle the weaknesses of earlier generations. This paper presents an advanced compact L-shaped two-port MIMO antenna array that offers wideband performance, high isolation without using any decoupling structure, and low ECC for millimeter-wave (mm-wave) 5G systems. With a bandwidth equal to 13.9 GHz and a high gain of 6.9 dB, and is designed to operate in the frequency range from 26.1 GHz to 40 GHz. A compact and efficient MIMO structure is produced by placing the antenna elements orthogonally, which reduces mutual coupling. The proposed array is composed of two L-shaped antenna elements with a rectangular slot in a partial ground plane, each of them being built on a 0.254 mm thick Rogers RT5880 (lossy) substrate. The MIMO antenna array is 16 × 27 mm^2 in size, which shows a 33–70% reduction in size compared to recent wideband counterparts. The array design exhibits improved performance as the gain increases to 6.2 dBi and a radiation efficiency of over 95% across the operating band. It is discovered that there is less than -15 dB of isolation between the elements. Total active reflection coefficient (TARC) is less than −10 dB, is approximately 10 dB, channel capacity loss (CCL) is less than 0.1 bits/sec/Hz, and ECC < 0.001 is among the major MIMO performance parameters that are well within the optimal range, demonstrating a measurable and balanced trade-off between compactness and performance. The proposed design is compact and has high bandwidth without compromising performance, unlike previous designs in which improvement in one parameter often led to degradation in another. The aforementioned results confirm that the proposed design is suitable for next-generation millimeter-wave wireless communication systems.

Keywords: 5G, MIMO, Antenna Array, Mm-Wave, CCL

Introduction:

As mobile phones progress toward becoming an integral and indispensable aspect of daily life, they have dramatically improved our operational capacity, convenience, and interactivity through internet connectivity. This increasing dependence has generated considerable interest in the telecommunications community. The 2020 Cisco Visual Networking Index report estimates that the video streaming era requires high bandwidth and non-stop data flows. Video traffic alone grew to 73% of overall internet traffic in 2016 and was forecast to hit 82% by 2021. Additionally, it was predicted that between 2016 and 2020, traffic associated with virtual reality and augmented reality would increase twentyfold, whereas live internet video traffic was expected to rise fifteen times over the same period. With this increase in reliance on mobile devices, mobile data traffic has also increased exponentially [1]. All these technological achievements mark a paradigm shift towards more complex wireless communication systems. As such, high data rates, better spectral efficiency, minimized mutual coupling effects, trustworthy signal transmission, and high-speed connections are in critical demand, which existing communication systems are increasingly failing to meet [2][3][4][5].

There is no unique definition or one-size-fits-all architecture of a 5G antenna; instead, it arises from the blend of various techniques, arrangements, and conditions in order to fulfill the required system conditions [6]. To cater to the need for improved data rates and enhanced spectral efficiency, this paper investigates utilizing the under-utilized mm Wave band between 30 GHz and 300 GHz. Nevertheless, working at these high frequencies contributes significantly to path loss and signal attenuation, such that stable communication becomes difficult in 5G services. Atmospheric conditions further aggravate the problems, as they have an significant effect on mm-wave signal propagation [7]. A 2-port MIMO antenna with the incorporation of a complementary split ring resonator in the ground plane was designed, but the achieved bandwidth is very low [8].

In [9] a compact quad-port MIMO antenna with a hybrid decoupling structure is designed, which gives very high gain, but the bandwidth is compromised, which is 7.2 GHz. To meet the demand for higher data rates, an innovative design was developed with a compact size, but it did not succeed in achieving high gain and broad bandwidth [10]. In [11] a 79% efficient circular microstrip patch antenna with FR-4 substrate and relative permittivity of 4.4 is designed to decrease antenna size for WLAN by introducing slots in the patch itself. In [12], a design is presented where 20 dBi and 8 dBi are the gains over the range of 24 GHz - 40 GHz. This paper proposed an orthogonal two-port MIMO antenna array in order to reduce the inter-element coupling experienced in 5G mm-wave applications. Two operational bands at 28 GHz and 38 GHz were considered, with the antenna designed to operate over 27–40 GHz. The antenna was fabricated on an FR-4 substrate because it was cheaper and easier to fabricate.

Achieving high isolation is one of the significant problems of MIMO antenna systems in degrading system performance. It can be overcome by using Electromagnetic Band Gap (EBG) structures [13], which ensure in-phase reflection and high surface impedance, thus enhancing isolation. Out of many isolation improvement techniques, arranging antenna elements in orthogonal locations is promising by enhancing gain and attaining system efficiency of over 95% [14].

A high-gain MIMO antenna with double operating bands, 27.1 GHz - 28.71 GHz for the 28 GHz band and 36 GHz – 42 GHz for the 38 GHz band, has been designed in [15], albeit at the cost of bandwidth. Similarly, [16] presents an eight-element MIMO antenna array wherein elements are located on opposite sides to provide high isolation without employing any decoupling structure, though with restricted bandwidth performance. An anti-parallel ultra-wideband (UWB) antenna is designed in [17] featuring high gain in a compact size. Yet, its bandwidth of 34.1 GHz –39.7 GHz is still a bottleneck.

In [18], a very compact antenna of size 2.62 mm × 2.62 mm was designed for 5G by using parasitic elements operating at both 28 GHz and 38 GHz. Further reduction in mutual coupling was achieved by [19] where a rectangular slot has been engraved into the ground plane along with additional design modifications. On the other hand, [20] presented a four-element MIMO antenna array using the defected ground structure (DGS) for ultra-wide bandwidth starting from 25.66 GHz to 41.74 GHz. The antenna was designed horizontally oriented, and the spacing between elements was appropriate, so no other decoupling structure was used.

A two-port MIMO antenna is proposed for 5G applications performing in the mm-wave band, particularly at 28 GHz. Rogers RT5880. This consists of a novel L-shaped antenna design that exhibits very low mutual coupling and high isolation. All the significant parameters needed for good MIMO performance are improved, including TARC, ECC, CCL, and gain, while retaining compactness.

The main aim of this research is to optimize the balance between structural compactness and performance. The recommended antenna design exhibits high gain and broadband behavior while maintaining enhanced MIMO performance parameters, hence being a very suitable option for future 5G wireless systems.

There are four sections in the research paper. The introduction is given in Section 1, and the proposed antenna's design process is described in Section 2. The results are covered in Section 3, and the paper's conclusion is covered in Section 4.

Section II: Design And Methodology:

Single Element Design:

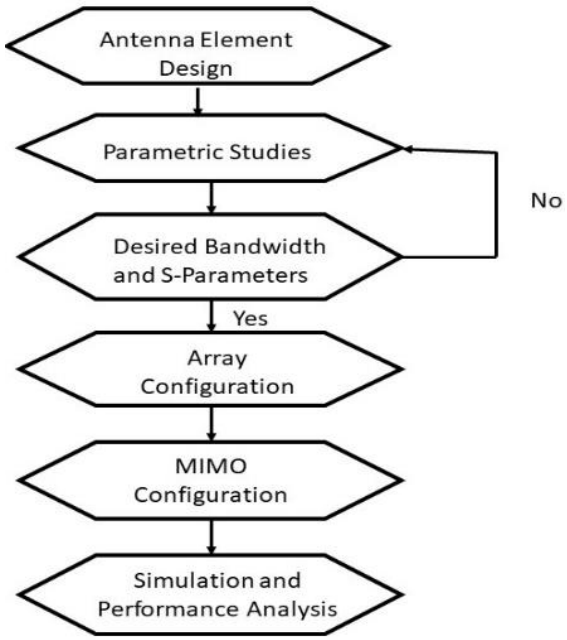

Figure 1. Flow Diagram of Antenna Design

The Rogers RT5880 substrate, which was selected for its low-loss properties and suitability for high-frequency applications, is used in the design of the antenna. The substrate's dielectric constant is 2.2, its height is 0.254 mm, and its loss tangent is 0.0009. CST, a commercially available electromagnetic simulation program, is used to design and simulate the antenna.

These four steps are followed to achieve the resonance frequency for wideband applications in a wireless communication environment.

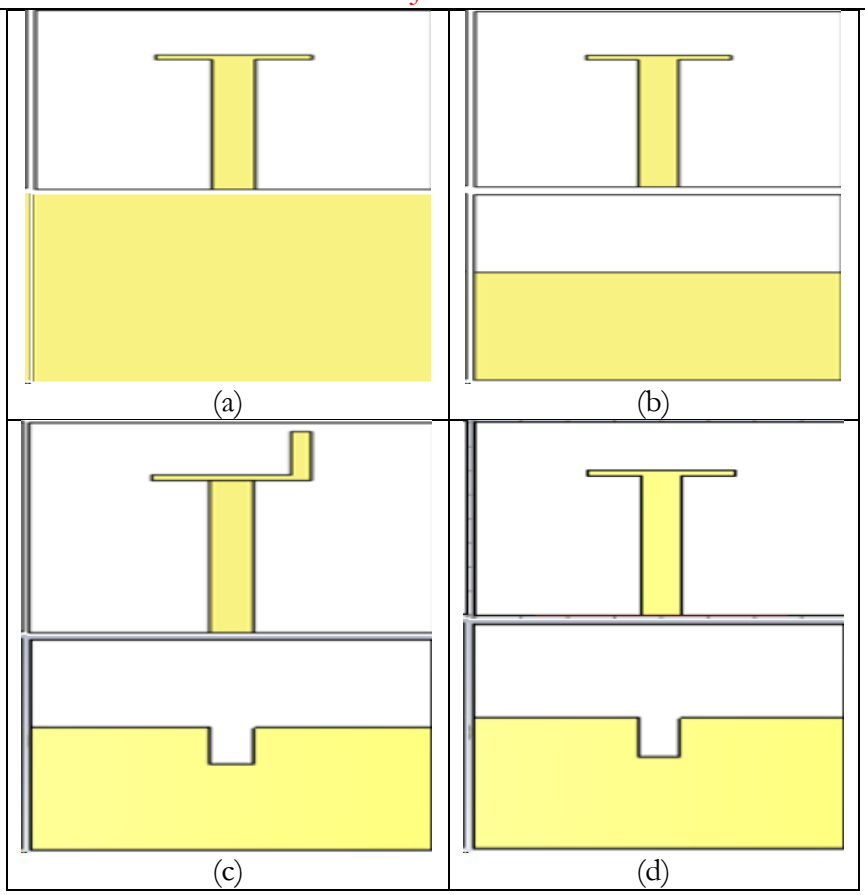

Figure 2. Single-element design steps (a) First step, (b) Second step, (c) Third step, (d) Fourth step

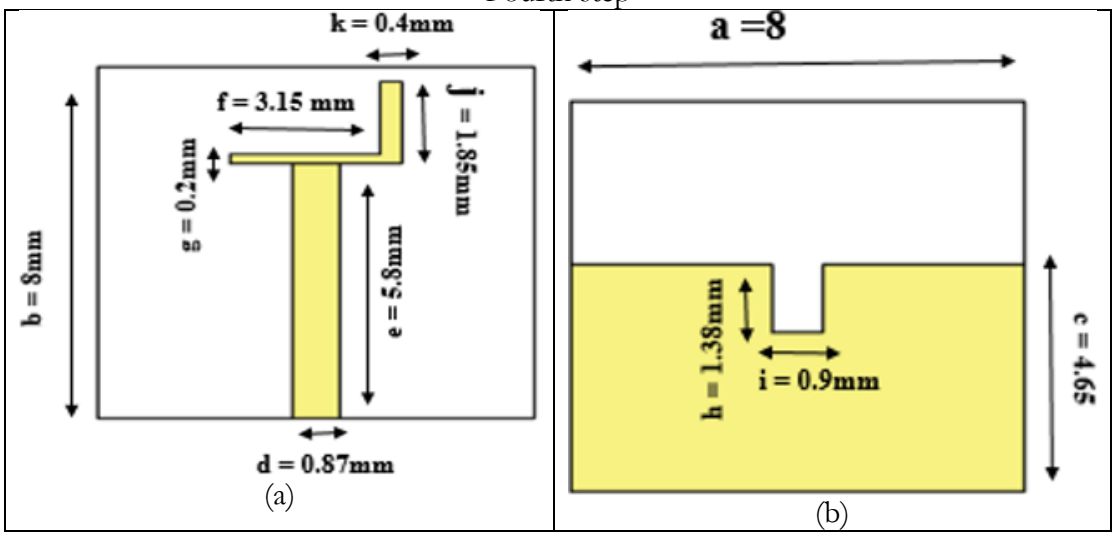

Figure 3. Single element design (a) top view (b) bottom view with rectangular slot in truncated ground

In order to determine the impedance matching and resonant frequency, the patch antenna length and width were used. The following are the equations used to calculate the length and width of the patch.

$$W_p = \frac{c}{f_c}\sqrt{\frac{\varepsilon_r+1}{2}} \quad (1)$$

$$\varepsilon_{eff} = \frac{\varepsilon_r+1}{2} + \frac{\varepsilon_r-1}{2}\left(1+\frac{12h}{W_p}\right)^{-1/2} \quad (2)$$

$$\Delta L = 0.421h\frac{(\varepsilon_{eff}+0.3)\left(\frac{W_p}{h}+0.264\right)}{(\varepsilon_{eff}-0.258)\left(\frac{W_p}{h}+0.8\right)} \quad (3)$$

$$L_{eff} = \frac{c}{2f_\circ\sqrt{\varepsilon_{eff}}} \quad (4)$$

$$L_p = L_{eff} - 2\Delta L \quad (5)$$

Where L_p and W_p is the length and width of the patch, h is the height of the substrate, c is the speed of light, ε_r is the relative permittivity, ε_{eff} is the effective permittivity, ΔL is the length extension, L_{eff} is the effective length, f_c is the central frequency, $f_\circ$ is the resonant frequency.

Table 1. Optimized Parametric table

Parameters	Hs	a	b	c	d	e	F	g	h	i	j	K	
Value(mm)	0.254	8	8	6.65	0.87	5.8	3.15	0.2	1.38	0.9	1.85	0.4	
m	n	o	p	$a_{50\Omega}$	$d_{100\Omega}$	A	B	C	D	E	F	G	H
7.98	1.8	1.06	7.1	0.9	0.26	5	8.5	1	16	11	3.55	6.65	27

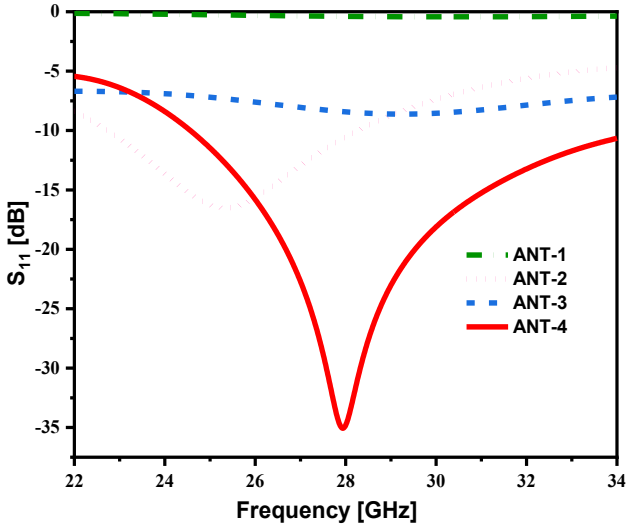

Figure 1. Simulated Reflection coefficient of 1st, 2nd, 3rd and 4th step of Single Antenna

The evolution model of antenna design is shown in Figure 2 along with its S11 Parameters as shown in Figure 4, which indicates the working of the antenna at different stages of design. Figure 3 depicts the progressive development of the antenna under consideration, while Figure 4 shows the corresponding reflection coefficient.

The original patch antenna in Figure 2(a) has weak impedance matching, represented by a poor S11 response. The ground plane is truncated as depicted in Figure 2(b) to enhance matching and resonance according to the larger S11 dip. Inserting a rectangular slot in the ground in Figure 2(c) provides a slight improvement. The last L-shaped patch design in Figure 2(d), however, demonstrates significant improvement in matching impedance and frequency range, with a distinct, deep S11 resonance in Figure 4, validating the optimized function of the antenna for high-frequency systems. The evolution of the antenna design shown in Figure 2 is also confirmed through the surface current density in Figure 5. In the initial stage of design, as represented in Figure 2(a), the current distribution in Figure 5(a) is weak and non-uniform, reflecting poor radiation. With ground truncation, as described in Figure 2(b), the current focuses more along the radiating edges, as demonstrated in Figure 5(b), verifying enhanced radiation efficiency. By including a rectangular slot in the ground plane, as in Figure 2(c), the current distribution shows slight variations, as illustrated in Figure 5(c). In the final

configuration of the antenna design, Figure 2(d) presents an L-shaped patch with high and uniform current concentration along the entire radiating surface, as shown in Figure 5(d), thereby ensuring efficient radiation and confirming the optimized working of the design.

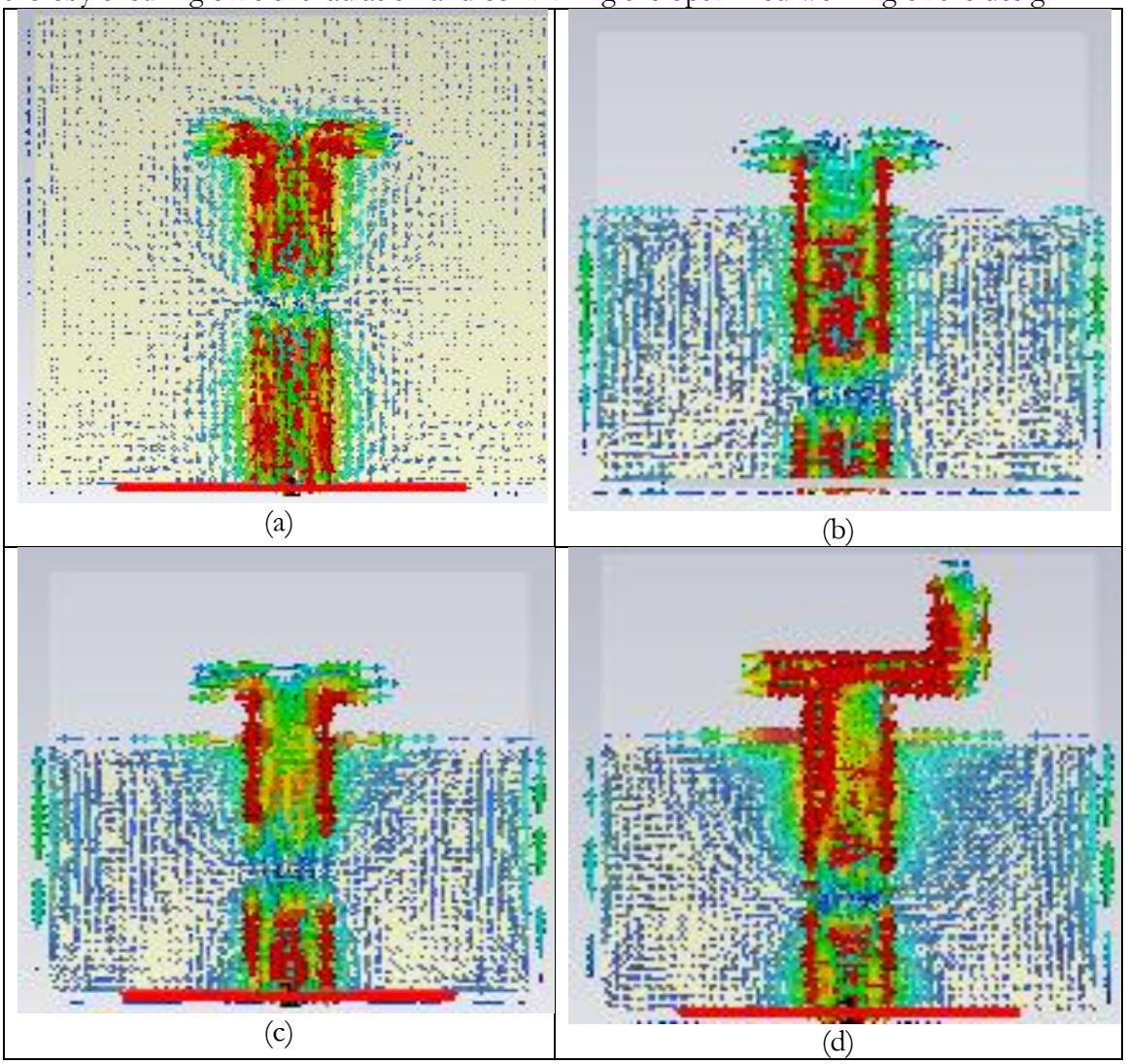

Figure 2. Surface Current Density at 28GHz of (a) First step, (b) Second step, (c) Third step, (d) Fourth step

Parametric Analysis:

Figure 6 shows the parametric analysis of the initial antenna design. To optimize performance, a parametric sweep is conducted for the ground slot, truncated ground length, feed width, and feed length. The parametric sweep for the feed width (Figure 6(a)) ranges from 0.8 mm to 0.92 mm with a step size of 0.03 mm. It shows satisfactory result for the value of 0.87mm. Similarly, the parametric sweep for the length of feed is shown in Figure 6(b) with a step size of 0.25, which shows a satisfactory result for impedance matching at a value of 5.8mm. The length of the ground is checked for different values ranging from 3.65 to 7.65 as well, as shown in Figure 6(c). Finally, different values ranging from 0.9 to 1 are checked for the ground slot to optimize the results for the proposed design, as shown in Figure 6(d).

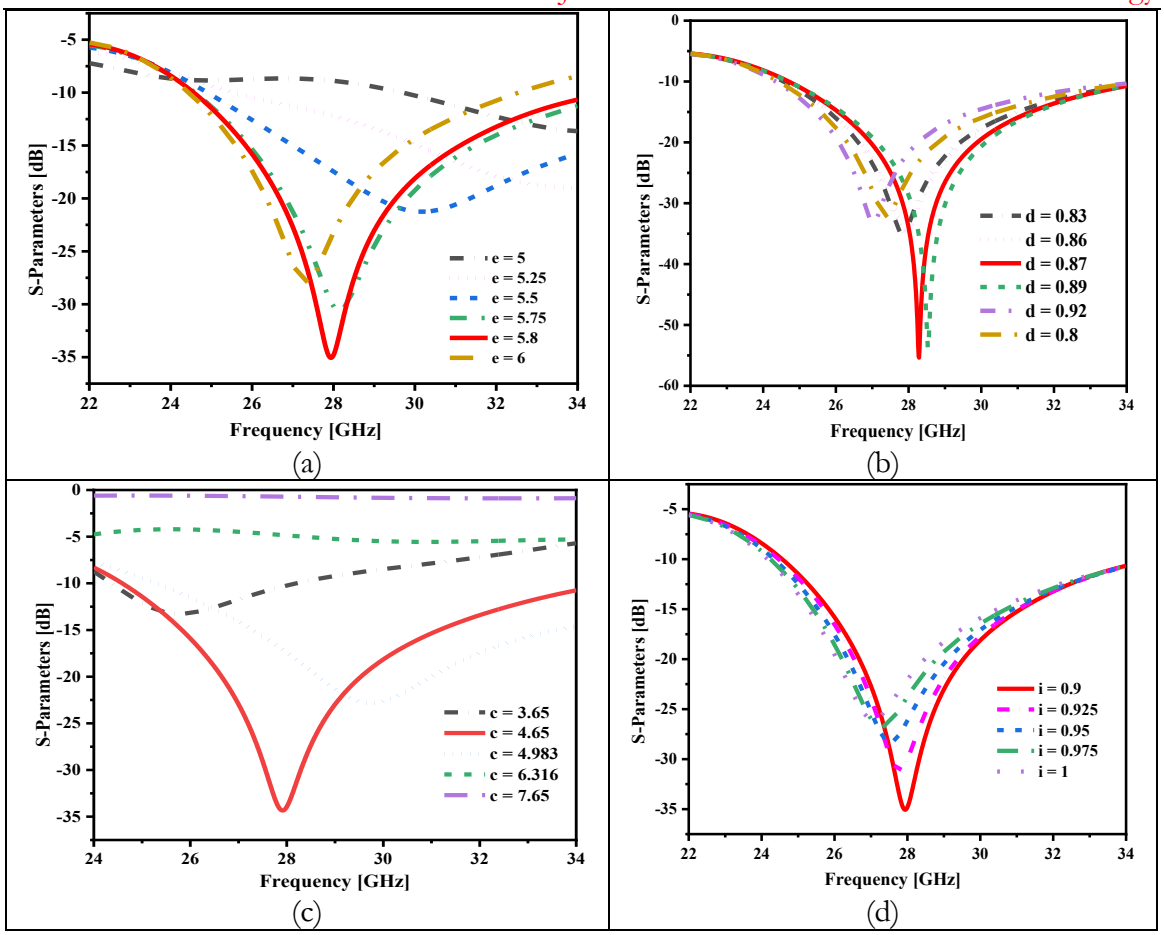

Figure 3. Optimized Parametric analysis (a) width of feed (b) length of feed (c) length of ground (d) ground slot

This study shows that for better performance, it is necessary to fine-tune different values and then select the best value.

Antenna Array Design:

5G applications often start with a single-element antenna design, which provides a low gain of 4.5 dB and operates at 28 GHz. The gain achieved is not satisfactory for operations in mm-wave wireless communication. Therefore, there is a critical need for improvement in gain. One such technique is the use of array configuration [21] where multiple antennas are transformed into an array and the power supply is through a single feed. The proposed antenna design is converted into a network using corporate feeding, which consists of two antenna elements forming a 1×2 array, in order to increase the gain at the selected frequency of interest from 3.4dBi. When the primary 50Ω feed is split into a 100Ω track impedance, the array network is transformed as shown in Equation 6. While the main feed line's width is adjusted to achieve an impedance of 50 Ω, the feed line width for the other transmission lines is adjusted to achieve an impedance of 100 Ω. Figure 7 shows the 1x2 array antenna with a single computed antenna dimension in the proposed design. The top and bottom views of the suggested array are depicted in Figures 7(a) and 7(b), respectively. The same measurements used for a single antenna element are used to optimize the array's power distribution.

$$W_z = \left(\frac{377}{zo\sqrt{\varepsilon_r}} - 2\right) \text{x } h_s \quad (6)$$

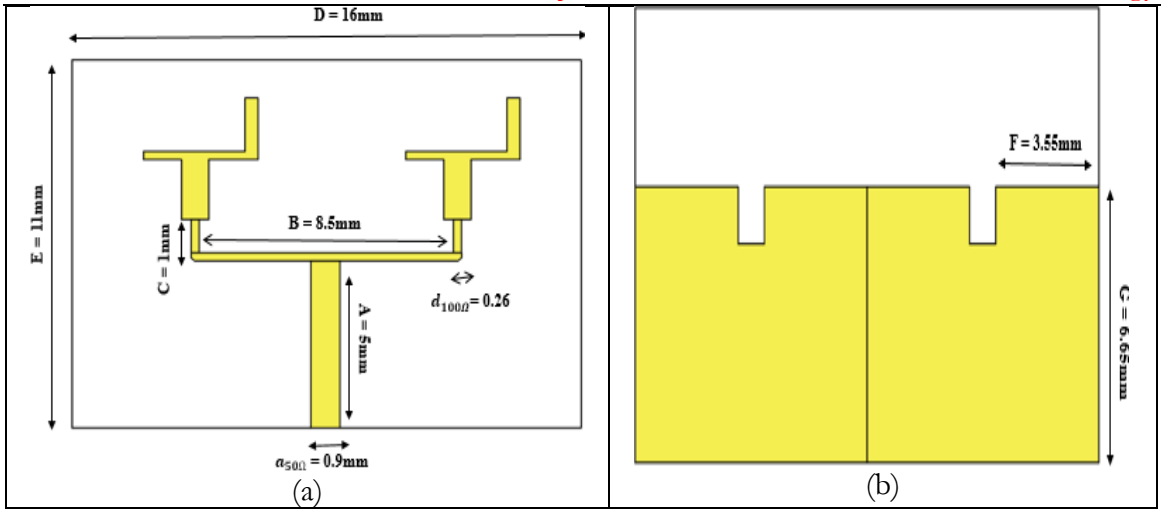

Figure 4. Proposed Corporate Antenna Array (a) top view (b) bottom view

The reflection coefficient for a 1×2 array is presented in Figure 8. The bandwidth for a 1x2 array is from 27.1 GHz to 40 GHz, which is high in comparison to a single element.

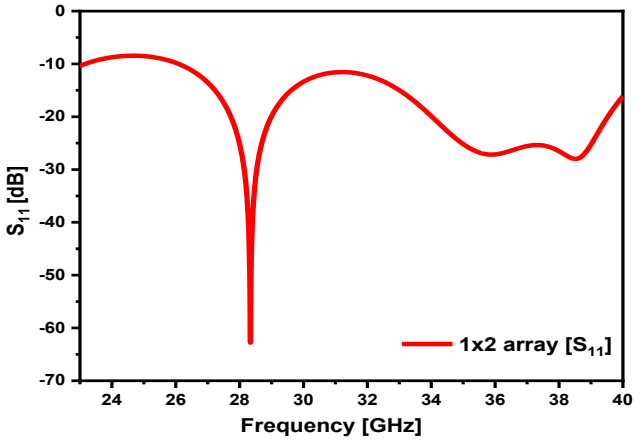

Figure 8. Reflection Coefficient of Antenna Array

Figure 9 depicts the array's gain characteristics, which demonstrate a significant increase in gain up to 6.2 dB over the single element configuration. The gain has increased from 4.5 dB to 6.2 dB when a single element was transformed into an array. This is consistent with the array configuration, and due to inter-element spacing, the array maintains compactness while preserving wide bandwidth.

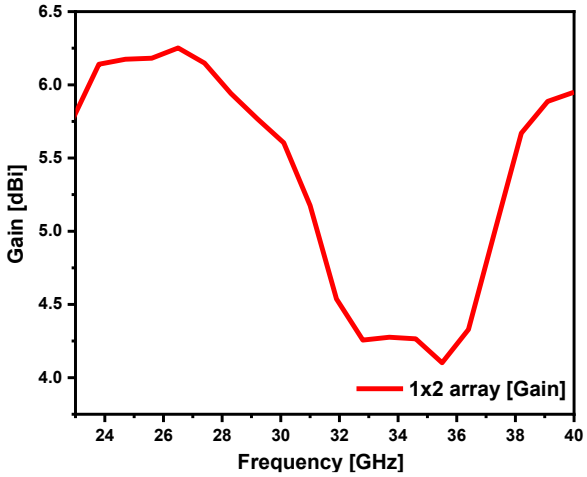

Figure 9. Gain of Array

2-Port MIMO Configuration:

Figure 10, given below, shows the extended version of the array, which is evolved into a 2-port MIMO antenna. The arrays are placed orthogonally with a 90° rotation, which reduces mutual coupling and improves isolation. As for transformation into an array, multiple antennas are used, which use a single port. This harms channel capacity. To address this adversity, multiple ports are used. Although it is very easy to use this technique when a single antenna is handling, the problem of mutual coupling arises when the array is transformed into MIMO. As a result, the overall dimensions of the MIMO antenna are 16 mm by 23 mm.

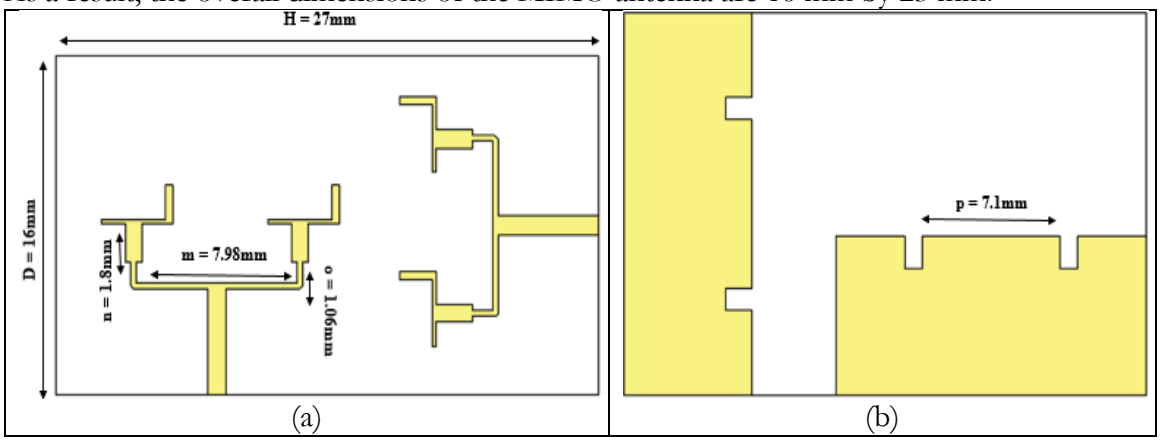

Figure 5. Proposed MIMO Antenna (a) top view (b) bottom view

S-Parameters and Mutual Coupling of MIMO Antenna:

The reflection efficiency (S-parameters) of the designed 2-port MIMO antenna is shown in Figure 11. The return loss values (S11 and S22) remain below −10 dB throughout the range of frequencies in which the antenna operates. This indicates proper impedance matching; therefore, resulting in minimal reflection at each port. The significant dips in the S11 and S22 curves at several frequencies mean that the antenna radiates efficiently over a large frequency range, with many different resonation points. The resemblance in the reflection responses in both ports guarantees uniform impedance behavior, which is of prime importance for stable MIMO performance in the millimeter-wave regime. Figure 12 depicts the isolation characteristic of the designed MIMO antenna for a visual indication of the correlation between ports one and two. The isolation levels are very low, with a value of less than −15 dB for both ports.

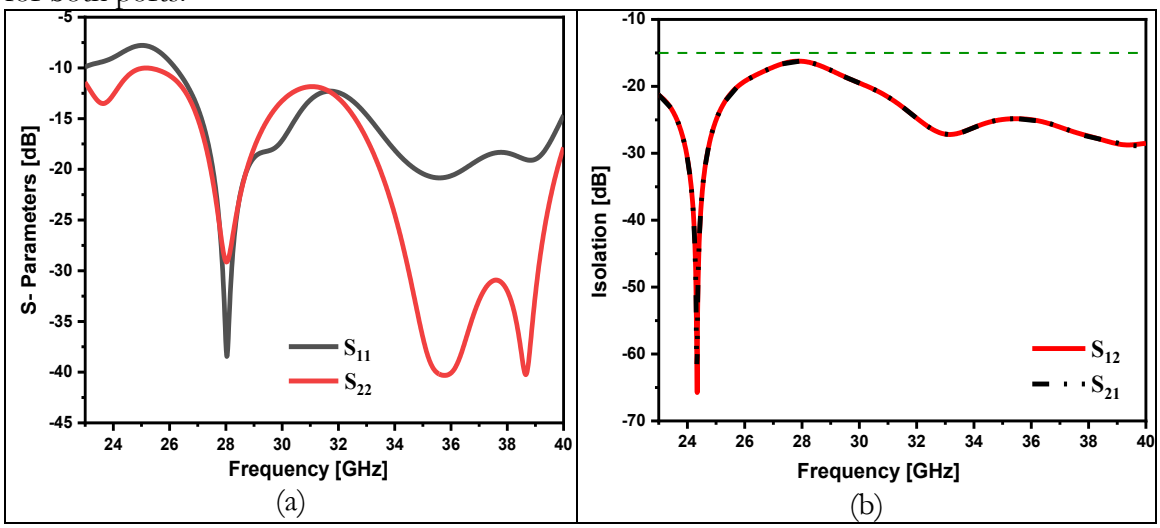

Figure 11. Simulated results of 2-port MIMO Antenna (a) S-Parameters (b) Isolation Coefficient

Section III: Simulations and Results:

Surface Current Density:

The existing distribution in Figures 12(a) and 12(b) at 28 GHz illustrates the mutual coupling behavior of the antenna elements when both ports are separately excited. In both cases, it can be observed that the radiated fields are mainly directed in a direction away from the adjacent element with little overlap among the radiation lobes. This clearly shows high isolation between the ports. The S12 is -18 dB at 28 GHz. It should be noted, however, that a negligible coupling has been obtained without adding a decoupling structure, since the element layout and orientation automatically provide sufficient spatial separation. The fact that there is minimal or no field interaction in the element space is a surety that mutual coupling is inherently suppressed, and no additional decoupling elements are necessary. It further enables the efficient and reliable operation of MIMO systems, yielding a simplified antenna design.

For Port 1 and Port 2 excitations at 34 GHz, the current distributions in Figures 12(c) and 12(d) show significant current focus on the individual active elements, confirming efficient excitation and radiation. The S12 is -21 dB at 34 GHz. In both cases, there is little induced current on the non-excited element, showing better isolation and low mutual coupling. Current remains well-confined at the patch edges and feed lines. This would suggest good impedance matching, hence effective design. This port symmetry justifies the antenna's use for MIMO operation at 34 GHz with stable radiation and good port-to-port isolation. In addition to qualitative surface current observations, mutual coupling is quantified through the transmission coefficient. The S12 remains below -15 dB while further reducing at resonating frequencies 28 GHz and 34 GHz. Moreover, the low induced current magnitude on the non-excited element is consistent with the measured isolation and indicates suppressed near-field coupling.

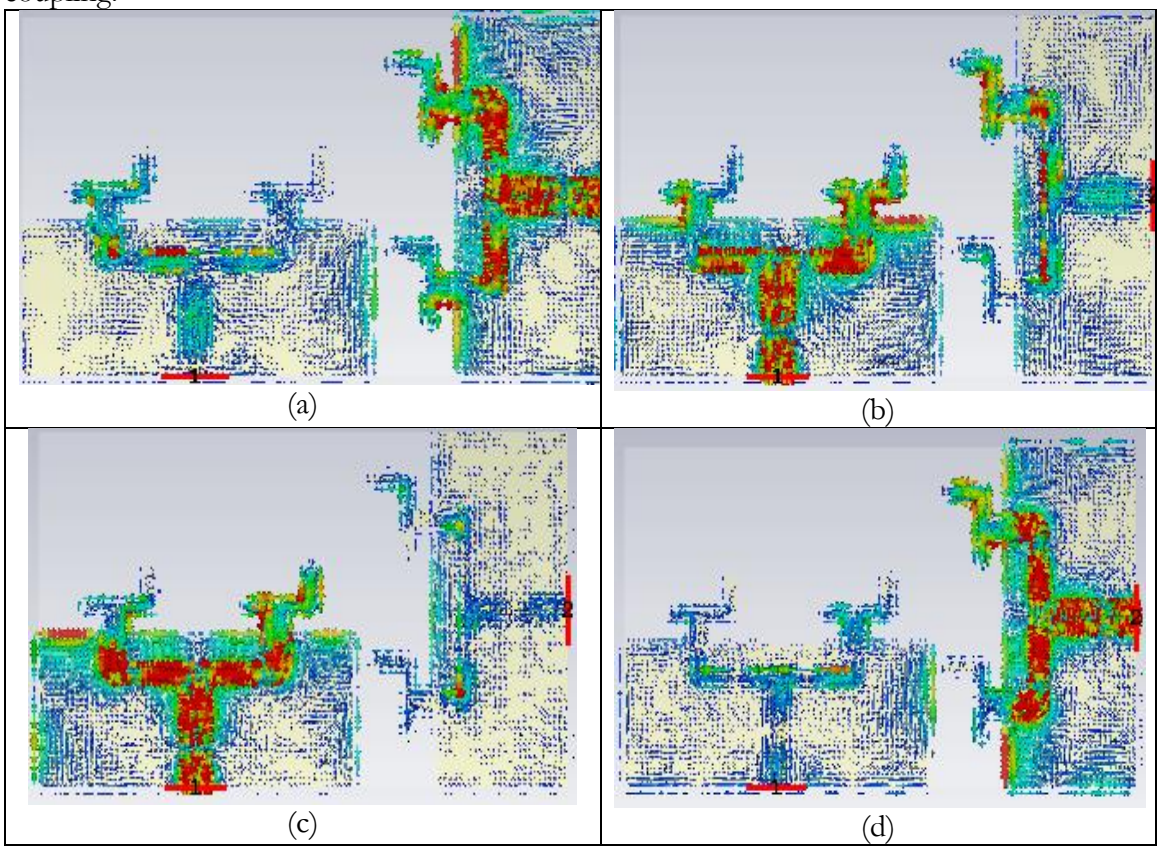

Figure 12. Current Distribution of MIMO Antenna Array at 28GHz (a) excitation at port 1 (b) excitation at port 2, At 34 GHz (c) excitation at port 1 (d) excitation at port 2

Far Field Measurement:

The characteristics of the proposed MIMO antenna, such as gain and radiation patterns, are assessed over its operational broadband frequencies (i.e., 28GHz, 31GHz, 34GHz) to determine their overall effectiveness. At 28 GHz, as depicted in Figure 13(a), it has a wide main lobe with good directivity, indicating adequate coverage. At 31 GHz, in Figure 13(b), the radiation is more concentrated with a thin beam and better gain, hence showing higher directionality. In Figure 13(c), symmetrical and stable radiation with low side lobes is observed at 34 GHz, demonstrating consistent performance. These results demonstrate that the antenna is suitable for for high-frequency applications like 5G and mm-wave communication.

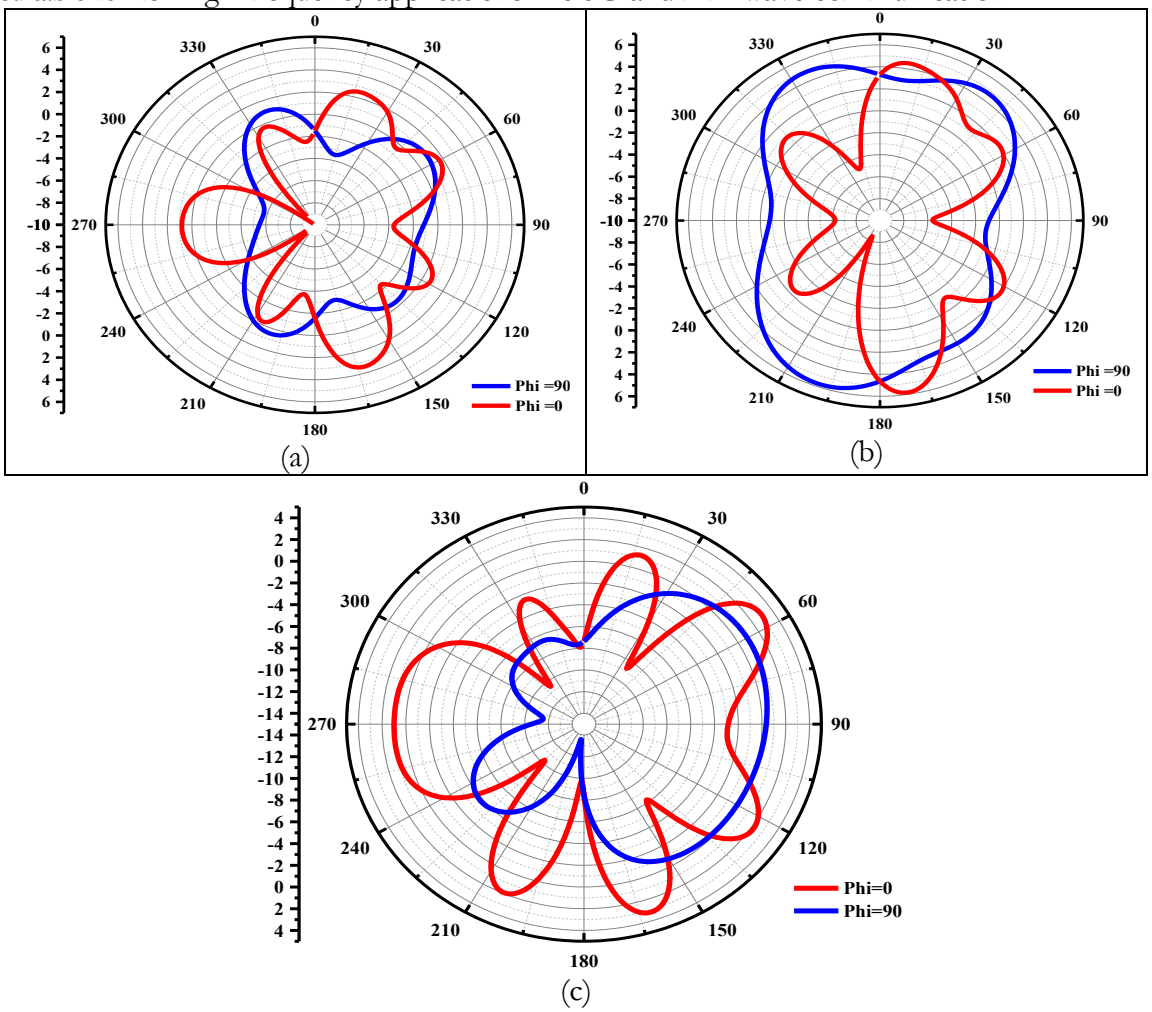

Figure 6. Radiation Pattern of MIMO Antenna (a) 28GHz (b) 31GHz (c) 34GHz

Gain and Efficiency:

In Figure 14, the gain of the MIMO antenna design is shown. The highest gain is approximately 6.9 dBi, greater than other designs, but also with a considerable gain of approximately 6.5 dBi at 28 GHz. The MIMO design also maintains a high radiation efficiency ranging from 0.85 to 0.95, indicating minimal power loss and good impedance matching throughout the band. Such stability in the efficiency, coupled with the increased gain, confirms the robustness of the MIMO design for wideband and millimeter-wave communications.

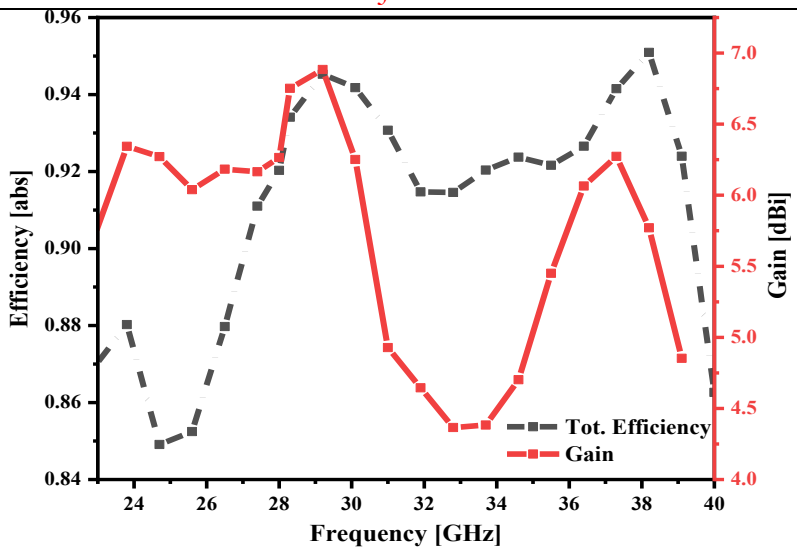

Figure 7. Gain and Efficiency of MIMO Antenna

Mimo Antenna Performance:

In MIMO technology, multiple antennas are employed to evaluate performance using metrics such as Total Active Reflection Coefficient (TARC), Envelope Correlation Coefficient (ECC), Channel Capacity Loss (CCL), Diversity Gain (DG), Mean Effective Gain (MEG), along with standard parameters like radiation efficiency, bandwidth, gain, and efficiency [22][23]. These metrics are utilized to assess the performance of the proposed MIMO antenna array.

Total Active Reflection Coefficient

For an MIMO antenna, the TARC [24] is given by

$$TARC = \sqrt{\frac{\left(|S_{11}+S_{12}e^{j\Theta}|^2+\left(|S_{21}+S_{22}e^{j\Theta}|^2\right)\right)}{2}} \quad (7)$$

Contrary to the existing antenna, in the proposed antenna design, the TARC always remains below -10 dB, as shown in Figure 15 below. This indicates a low reflection coefficient, which signifies efficient power transfer and confirms that the antenna operates properly in the desired frequency range.

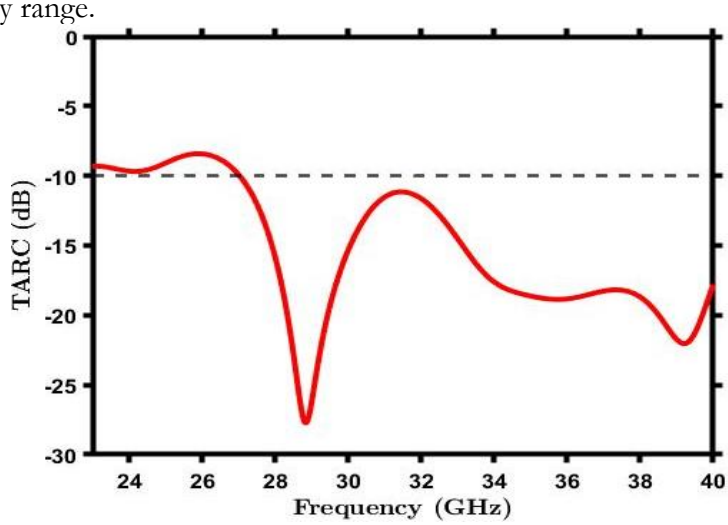

Figure 8. Total Active Reflection Coefficient of Proposed MIMO Antenna Array

Envelope Correlation Coefficient:

To achieve the best diversity characteristics, the signals received at the destination receiver must be as uncorrelated as possible. Signal independence is measured by using the

Envelope Correlation Coefficient (ECC), as described in [25]. This calculation is typically done using far-field radiation.

$$ECC = \frac{|S_{11}S^*_{12}+S_{21}S^*_{22}|^2}{(1-|S_{11}|^2-|S_{21}|^2)(1-|S_{22}|^2-|S_{12}|^2)} \quad (8)$$

Figure 16 shows the ECC variation over the operating bandwidth. From Figure 16, it can be seen that the ECC is below 0.001 over the entire frequency range. This implies that the isolation between antenna elements is excellent, and the correlation between radiators is very low. The presented design is thus very suitable for future mm-wave wireless communication and gives reliable performance with high data throughput.

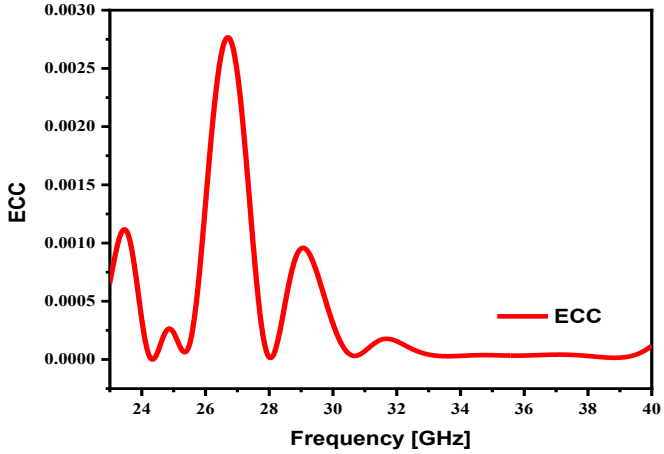

Figure 9: Envelope Correlation Coefficient of Proposed MIMO Antenna Array

Channel Capacity Loss:

CCL is an important parameter that reflects the efficiency of data transmission at frequencies within the operation range through a MIMO system.

$$CCL = -log_2 \det(a) \quad (9)$$

A CCL of 0.4 bits/sec/ Hz [26] is normally considered to reflect good data transmission. In the proposed design, the CCL remains below 0.1 bits/sec/Hz across the whole operating band, as shown in Figure 17. The consistently low CCL obtained is demonstrates the design's effectiveness in supporting a robust and lossless data transfer capability.

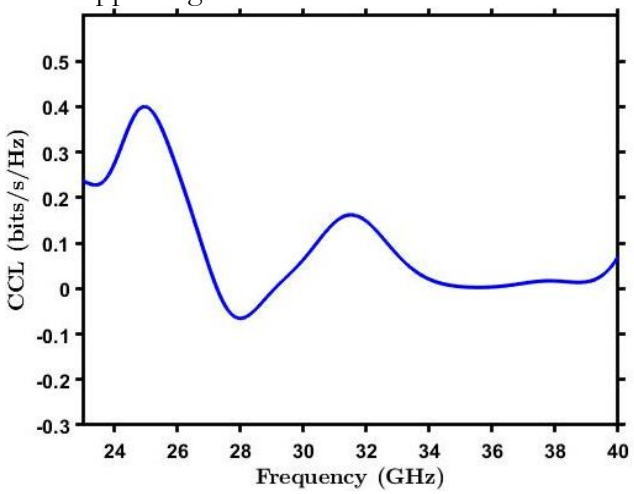

Figure 10. Channel Capacity Loss of Proposed MIMO Antenna Array

Diversity Gain:

Diversity gain (DG) is one of the main parameters in MIMO systems, and it characterizes how much SNR improvement [27] is obtained at the output of the diversity combiner. It reflects the ability of the system to enhance signal reliability by means of several antennas and is usually expressed through the ECC as:

$$DG = 10\ (\sqrt{1 - ECC^2} \quad (10)$$

As indicated in Figure 18, the DG value is practically equal to 10 within the operating band of frequency.

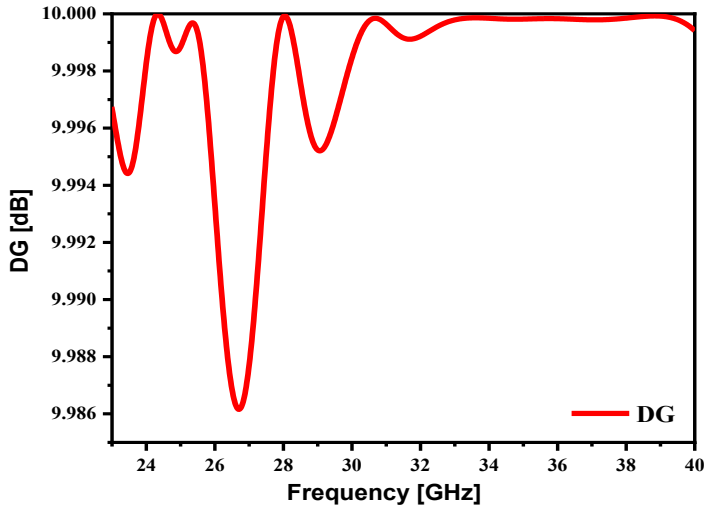

Figure 11. Diversity Gain (DG) Of MIMO Antenna Array

Discussion:

Table 2 also gives a comparative analysis of the suggested MIMO antenna and its predecessors' designs, clearly demonstrating the superiority of the suggested structure in terms of wideband operation, high gain, and enhanced isolation. The Rogers RT5880 substrate, which has small dimensions of 6 × 17.37 mm², was used in a compact ultra-wideband MIMO antenna that was reported in [17]. Although it had outstanding isolation, its bandwidth was severely constrained. Similarly, in [28], a 12 × 6 mm² antenna operating between 24 GHz and 30.25 GHz was able to achieve high isolation of -29 dB with the aid of a C-shaped decoupling structure, but the bandwidth enhancement was still negligible.

Although a high-gain and high-isolation MIMO antenna array was proposed in [29], its application range was limited due to its narrow usable bandwidth (37.29 GHz –38.24 GHz) and the design compromises on compactness for high gain. Improved bandwidth (20 GHz–32 GHz) and gain (6.5 dB) were provided by a four-port MIMO antenna in [30], but its isolation level of 20 dB made it less appropriate for high-frequency or interference-sensitive applications.

Although the gain was only about 2.8 dB, MIMO techniques were used in [31] to reduce multipath fading and achieve a wide bandwidth (2.9 GHz –18 GHz) in a structure that was 18 × 36 mm². In [32], yet another large MIMO design showed subpar overall performance in terms of isolation, gain, and bandwidth. The design put forth in [33] used a four-element configuration to target Ka-band short-range communication. however, its large 35 × 40 mm² size limits its practical application.

Additionally, there were performance issues with a two-element slot-loaded MIMO antenna in [34], especially with regard to bandwidth and gain. A large MIMO antenna with high gain was presented by [35], but it was not compact enough to be integrated into miniaturized platforms. Although the gain is very high, the design is bulky, which is not feasible for incorporating into portable devices. A four-port MIMO antenna in [36] had poor bandwidth performance but good gain and isolation.

The proposed MIMO antenna array in this study provides a more optimized and balanced solution in contrast to the earlier studies. This design is ideal for mm-wave and 5G applications since it offers high isolation levels while achieving a small form factor, greatly increased gain, and wide bandwidth.

Table 2. Performance Comparison of Proposed Design with Recent Literature

Ref	Size (mm) [Ports]	Frequency range (GHz) [bandwidth] (GHz)	Isolation (dB)	Peak gain (dBi)	ECC	DG	Fabricated material	TARC	CCL
[17]	6X17.37 (2)	34.1-39.7 [5.6]	-65	6.7	0.00035	9.99	Roger 5880	<-10dB	0.034
[28]	12x20 (2)	24-30.25 [6.25]	-29	9.25	0.005	9.99	Roger 6002	Within limits	<0.3
[29]	20x40 (2)	37.29-38.64 [1.35]	-40	12.8	<0.00014	9.99	Roger RT5880	<-10dB	<0.3
[30]	24x32 (4)	20-32[12]	-20	6.5	0.0055	9.99	RO5880	<10dB	<0.4
[31]	18x36 (2)	2.9-18 [15.1]	-18	>2.8	<0.05	9.95	FR4	<-10dB	<0.29
[32]	150x75 (8)	3.4-4.7 [1.3]	-11	>1.5	<0.08	10	FR4	<-10dB	<0.3
[33]	35x40 (4)	24.1-30.9 [6.8]	-30	6.5	<0.18	10	Roger RT5880	<-10dB	<0.25
[34]	39x31 (2)	30.2-40 [9.8]	-25	4.96	<0.0025	9.98	Roger RT5880	<-10dB	<0.3
[35]	55.27x27.635 (2)	27-40 [13]	-30	10	<0.0001	10	FR4	Within limits	<0.4
[36]	25x25 (4)	25.28-28.02 [2.74]	-23.2	8.72	<0.0015	9.99	Roger RT 5880	<-10dB	<0.4
Prop.Work	16x27 (2)	26.1-40 [13.9]	-15	6.9	<0.003	9.9	Rogers 5880	Within limits	<0.3

Conclusion:

This paper describes the development and simulation of a compact 2-port L-shaped MIMO antenna designed specifically for use in 5G millimeter-wave applications. The MIMO antenna has a peak gain of 6.9 dB across a frequency range of 26.1 GHz to 40 GHz with an overall total usable MIMO bandwidth of 13.9 GHz. Due to the perpendicular placement of the individual MIMO antenna elements, the amount of mutual coupling (or isolation) achieved by this design is greater than -15 dB with no additional decoupling components required between the individual antennas, but it can be further improved by introducing a decoupling technique. The major performance criteria for MIMO antennas indicate that the values for ECC (<0.001), DG (around 10 dB), TARC (< -10 dB), and CCL (< 0.1 bits/sec/Hz) are all well within standard specifications and therefore conclusively demonstrate that this design is feasible for MIMO antenna applications operating at high frequencies. The gain and data speed can be increased by increasing the number of ports. This design can be validated by fabricating and testing its performance in real-world scenarios. The performance of the MIMO antenna can be improved by introducing a decoupling structure.

Acknowledgment:

The authors acknowledge with gratitude the useful supervision, persistent encouragement, and constructive feedback given by Dr. Shahid Bashir, under whose supervision this research was successfully executed. The authors are also indebted to the [Electrical Engineering/University of Engineering and Technology Peshawar] for the facilities extended and support during this work.

References:

[1] C. R. Storck and F. Duarte-Figueiredo, "A Survey of 5G Technology Evolution, Standards, and Infrastructure Associated With Vehicle-to-Everything Communications by Internet of Vehicles," *IEEE Access*, vol. 8, pp. 117593–117614, 2020, [Online]. Available: https://ieeexplore.ieee.org/document/9125906

[2] André Noll Barreto, Bruno Faria, "5G – Wireless Communications for 2020," *J. Commun. Inf. Syst.*, vol. 31, no. 1, pp. 143–163, 2016, [Online]. Available: https://www.researchgate.net/publication/304532304_5G_-_Wireless_Communications_for_2020

[3] P. Patnaik, D. Sarkar, and C. Saha, "A Multi-band 5G Antenna for Smart Phones Operating at Sub-6 GHz Frequencies," *Proc. 2020 Int. Symp. Antennas Propagation, APSYM 2020*, pp. 32–35, Dec. 2020, doi: 10.1109/APSYM50265.2020.9350684.

[4] H. J. Nam, S. Lim, Y. J. Yoon, and H. Kim, "Tunable Triple-Band Antenna for Sub-6 GHz 5G Mobile Phone," *2020 IEEE Int. Symp. Antennas Propag. North Am. Radio Sci. Meet. IEEECONF 2020 - Proc.*, pp. 1455–1456, Jul. 2020, doi: 10.1109/IEEECONF35879.2020.9330484.

[5] J. Jiang and Y. Li, "A Wideband Kanji Patch Antenna for 5G Sub-6-GHz Applications," *2020 13th UK-Europe-China Work. Millimetre-Waves Terahertz Technol. UCMMT 2020 - Proc.*, Aug. 2020, doi: 10.1109/UCMMT49983.2020.9296092.

[6] Daniyal Ali Sehrai, Mujeeb Abdullah, "A Novel High Gain Wideband MIMO Antenna for 5G Millimeter Wave Applications," *Electronics*, vol. 9, no. 6, p. 1031, 2020, [Online]. Available: https://www.mdpi.com/2079-9292/9/6/1031

[7] A. A. Kiran Raheel, "E-Shaped H-Slotted Dual Band mmWave Antenna for 5G Technology," *Electronics*, vol. 10, no. 9, p. 1019, 2021, [Online]. Available: https://www.mdpi.com/2079-9292/10/9/1019

[8] N. Sheriff *et al.*, "Compact low-profile multiple-input multiple-output (MIMO) antenna for portable devices in next-generation 5G wireless networks," *Wirel. Networks 2025 316*, vol. 31, no. 6, pp. 4147–4161, Jun. 2025, doi: 10.1007/s11276-025-03991-7.

[9] Praveen Kumar, G.D. Goutham Simha, "High-isolation quad-port mmWave MIMO antenna with hybrid decoupling structure for V2V applications," *Results Eng.*, vol. 27, p.

106860, 2025, [Online]. Available: https://www.sciencedirect.com/science/article/pii/S2590123025029238

[10] A. Khabba, L. Sellak, J. Amadid, Z. El Ouadi, S. Ibnyaich, and A. Zeroual, "Innovative mm-Wave Compact Dual-Port MIMO Antenna with Inherent Wideband Isolation at 28 GHz for 5G Wireless Networks," *Signals Commun. Technol.*, vol. Part F3207, pp. 55–69, 2024, doi: 10.1007/978-3-031-56144-3_4.

[11] Chaitali Mukta, Mahfujur Rahman, "Design of a Compact Circular Microstrip Patch Antenna for WLAN Applications," *Int. J. AdHoc Netw. Syst.*, vol. 11, no. 3, pp. 1–11, 2021, [Online]. Available: https://www.researchgate.net/publication/353926912_Design_of_a_Compact_Circular_Microstrip_Patch_Antenna_for_WLAN_Applications

[12] K. S. Sultan and H. H. Abdullah, "Planar UWB MIMO-Diversity Antenna with Dual Notch Characteristicst," *Prog. Electromagn. Res. C*, vol. 93, pp. 119–129, 2019, doi: 10.2528/pierc19031202.

[13] M. A. T. Sakib, M. R. Islam, M. S. Islam, G. M. Asadullah, and M. S. R. Bashri, "Design of Quad Element MIMO Array with EBG Structure for Mutual Coupling Reduction," *Proc. 9th Int. Conf. Comput. Commun. Eng. ICCCE 2023*, pp. 405–409, 2023, doi: 10.1109/ICCCE58854.2023.10246046.

[14] I. Ahmad, Y. Liu, F. Wang, M. K. Khan, and M. M. Kamal, "Wideband MIMO Antenna System with High Inter-Elements Isolation for mm-Wave Communications and the Internet of Things (IoT)," *Prog. Electromagn. Res. Lett.*, vol. 124, pp. 37–45, 2025, doi: 10.2528/PIERL24112301.

[15] Mohammed Mahaboob Basha, Pendli Pradeep, Srinivasulu Gundala, Javed Syed, "Design of compact and high gain dual-band four-port MIMO antenna array for mm-wave 5G Communications," *Results Eng.*, vol. 25, p. 104153, 2025, [Online]. Available: https://www.sciencedirect.com/science/article/pii/S2590123025002415

[16] N. A. Abbasi *et al.*, "High-Isolation Array Antenna Design for 5G mm-Wave MIMO Applications," *J. Infrared, Millimeter, Terahertz Waves*, vol. 46, no. 1, pp. 1–22, Jan. 2025, doi: 10.1007/S10762-024-01027-3/TABLES/3.

[17] Ouafae Elalaouy, Mohammed EL Ghzaoui, Jaouad Foshi, "A high-isolated wideband two-port MIMO antenna for 5G millimeter-wave applications," *Results Eng.*, vol. 23, p. 102466, 2024, [Online]. Available: https://www.sciencedirect.com/science/article/pii/S2590123024007217

[18] H. T. Chou, B. A. Liu, S. C. Chen, and Y. J. E. Chen, "Dual-Band Dual-Polarized Microstrip Patch Antenna With Parasitic Elements for 5G Antenna-in-Package Design at Millimeter-Wave Frequencies," *IEEE Trans. Components, Packag. Manuf. Technol.*, vol. 13, no. 11, pp. 1778–1789, Nov. 2023, doi: 10.1109/TCPMT.2023.3321610.

[19] P. K. Desai and S. Bindu, "Design and Fabrication of a 2-Port Multiple Antenna System for mmWave Application," *J. Commun.*, vol. 18, no. 11, pp. 705–713, Nov. 2023, doi: 10.12720/jcm.18.11.705-713.

[20] Ashok Kumar, Ashok Kumar, Arjun Kumar, "Defected Ground Structure Based High Gain, Wideband and High Diversity Performance Quad-Element MIMO Antenna Array for 5G Millimeter-Wave Communication," *Prog. Electromagn. Res.*, vol. 101, pp. 1–16, 2023, [Online]. Available: https://www.jpier.org/issues/volume.html?paper=23030601

[21] N. Ojaroudiparchin, M. Shen, and G. F. Pedersen, "Beam-steerable microstrip-fed bow-tie antenna array for fifth generation cellular communications," *2016 10th Eur. Conf. Antennas Propagation, EuCAP 2016*, May 2016, doi: 10.1109/EuCAP.2016.7481156.

[22] P. N. Fletcher, M. Dean, and A. R. Nix, "Mutual coupling in multi-element array antennas and its influence on MIMO channel capacity," *Electron. Lett.*, vol. 39, no. 4, pp. 342–344, Feb. 2003, doi: 10.1049/el:20030219.

[23] R. G. Vaughan and J. B. Andersen, "Antenna diversity in mobile communications," *IEEE Trans. Veh. Technol.*, vol. 36, no. 4, pp. 149–172, 1987, doi: 10.1109/T-

VT.1987.24115.
[24] T. Pei, L. Zhu, J. Wang, and W. Wu, "A low-profile decoupling structure for mutual coupling suppression in mimo patch antenna," *IEEE Trans. Antennas Propag.*, vol. 69, no. 10, pp. 6145–6153, Oct. 2021, doi: 10.1109/TAP.2021.3098565.
[25] R. N. Tiwari, P. Singh, P. Kumar, and B. K. Kanaujia, "High Isolation 4-Port UWB MIMO Antenna with Novel Decoupling Structure for High Speed and 5G Communication," *2022 Int. Conf. Electromagn. Adv. Appl. ICEAA 2022*, pp. 336–339, 2022, doi: 10.1109/ICEAA49419.2022.9900029.
[26] Mahnoor Khalid, Syeda Iffat Naqvi, "4-Port MIMO Antenna with Defected Ground Structure for 5G Millimeter Wave Applications," *Electronics*, vol. 9, no. 1, p. 71, 2020, [Online]. Available: https://www.mdpi.com/2079-9292/9/1/71
[27] P. Garg and P. Jain, "Isolation Improvement of MIMO Antenna Using a Novel Flower Shaped Metamaterial Absorber at 5.5 GHz WiMAX Band," *IEEE Trans. Circuits Syst. II Express Briefs*, vol. 67, no. 4, pp. 675–679, Apr. 2020, doi: 10.1109/TCSII.2019.2925148.
[28] Wahaj Abbas Awan, Esraa Mousa Ali, "Enhancing isolation performance of tilted Beam MIMO antenna for short-range millimeter wave applications," *Heliyon*, vol. 9, no. 9, 2023, [Online]. Available: https://www.sciencedirect.com/science/article/pii/S2405844023071931
[29] Jalal Khan, Sadiq Ullah, "Design of a Millimeter-Wave MIMO Antenna Array for 5G Communication Terminals," *Sensors*, vol. 22, no. 7, p. 2768, 2022, [Online]. Available: https://www.mdpi.com/1424-8220/22/7/2768
[30] Hela Elmannai, Saad Hassan Kiani, B.G. Parveez Shariff, Daniyal Ali Sehrai, Tanweer Ali, Umair Rafique e, Abeer D. Algarni, "Design and characterization of a meandered V-shaped antenna using characteristics mode analysis and its MIMO configuration for future mmWave devices," *AEU - Int. J. Electron. Commun.*, vol. 186, p. 155477, 2024, [Online]. Available: https://www.sciencedirect.com/science/article/pii/S1434841124003637
[31] Shaik Kareemulla, Vijay Kumar, "Diversity performance of band notched ultra-wideband MIMO antenna," *Optik (Stuttg).*, vol. 272, p. 170128, 2023, [Online]. Available: https://www.sciencedirect.com/science/article/abs/pii/S0030402622013869
[32] Zhonggen Wang, Wenshi You, "Design of MIMO Antenna with Double L-Shaped Structure for 5G NR," *Symmetry (Basel).*, vol. 15, no. 3, p. 579, 2023, [Online]. Available: https://www.mdpi.com/2073-8994/15/3/579
[33] P. S. B. G, "High-Isolation Wide-Band Four-Element MIMO Antenna Covering Ka-Band for 5G Wireless Applications," *IEEE Access*, vol. 11, pp. 123030–123046, 2023, [Online]. Available: https://ieeexplore.ieee.org/document/10301425
[34] P. Tiwari, M. Kaushik, A. Shastri, and V. Gahlaut, "Two Element Microstrip-Fed Slot Loaded Millimeter Wave MIMO Antenna," *2023 Int. Conf. Adv. Technol. ICONAT 2023*, 2023, doi: 10.1109/ICONAT57137.2023.10080826.
[35] Amany A. Megahed, Ehab H. Abdelhay, Mohamed Abdelazim, Heba Y. M. Soliman, "5G millimeter wave wideband MIMO antenna arrays with high isolation," *EURASIP J. Wirel. Commun. Netw. Vol.*, vol. 2023, no. 61, 2023, [Online]. Available: https://link.springer.com/article/10.1186/s13638-023-02267-y
[36] S. E. B. K. Cem Güler, "A Novel High Isolation 4-Port Compact MIMO Antenna with DGS for 5G Applications," *Micromachines*, vol. 14, no. 7, p. 1309, 2023, [Online]. Available: https://www.mdpi.com/2072-666X/14/7/1309